# Implantable Antennas

*Asimina Kiourti and Konstantina S. Nikita*


Implantable medical devices (IMDs) are medical devices that are implanted inside the patient's body by means of a surgical operation and can be used for a number of diagnostic, monitoring, and therapeutic applications. Typical examples include implantable pacemakers, defibrillators, glucose monitors, cochlear implants, drug infusion pumps, intracranial pressure monitors, neurostimulators, etc. [1]. To be truly beneficial while preserving patient comfort, IMDs need to wirelessly exchange data with exterior monitoring/control equipment. Low-frequency inductive links have traditionally been used for wireless telemetry of IMDs [2], [3]. However, in an attempt to overcome their inherent limitations related to low data rate, restricted communication range, and sensitivity to intercoil misalignment, recent focus

*Asimina Kiourti (akiourti@biosim.ntua.gr) and Konstantina S. Nikita (knikita@ece.ntua.gr) are with the School of Electrical and Computer Engineering, National Technical University of Athens, Athens, Greece.*

*Digital Object Identifier 10.1109/MMM.2014.2308765*
*Date of publication: 7 May 2014*

is on antenna-enabled medical telemetry for IMDs. Wireless transmission is most commonly performed in the 402–405 MHz frequency band, which has been exclusively allocated for medical implant communications systems (MICSs), is internationally available and feasible with low-power circuits, falls within a relatively low-noise portion of the spectrum, and allows for acceptable propagation through human tissue [4]. Nevertheless, other radio-frequency (RF) bands might also be used, such as those defined in the recent IEEE 802.15.6 standard [5].

Implantable antennas, i.e., antennas that are integrated into RF-enabled IMDs, exhibit numerous challenges in terms of design, fabrication, and testing and are, therefore, currently attracting significant research attention [6], [7]. Numerical design of implantable antennas needs to be performed fast and in a way that optimally addresses issues related to miniaturization, exhibited radiation performance, patient safety, detuning phenomena, effect of the implantation site, etc. Furthermore, prototype fabrication of such miniature antenna structures is highly challenging given their critical tolerance to potential experimental versus numerical inconsistencies. Finally, in vitro and in vivo testing of implantable antennas is considered highly intriguing given the requirements for phantom formulation that matches the theoretical electrical properties and implantation inside living model animals, respectively.

The objective of this tutorial is to provide a simple, yet analytical and complete, step-by-step guide on the design, fabrication, and in vitro/in vivo testing of implantable antennas for medical telemetry applications. Simulations and experimentation are carried out within the framework of an MICS implantable patch antenna for intracranial pressure (ICP) monitoring applications. Nevertheless, challenges and suggested solutions are highlighted so that the presented methodologies and techniques can be applied to any implantable antenna model that the designer may have in hand.

## Selection of the Parametric Implantable Antenna Model

The first step in implantable antenna design is the selection of the intended antenna model. The selected antenna model should take into account considerations related to 1) miniaturization, 2) biocompatibility, and 3) prototype fabrication, as summarized in the following. Furthermore, it should be extensively parameterized to allow for a high number of degrees of freedom in the design. It is worth noting that patch designs are most commonly selected for implantable antennas because they are highly flexible in design, shape, and conformability [8]. Moreover, circular structures are very often preferred in an attempt to avoid sharp edges, which may hurt the surrounding biological tissues [9].

### *Miniaturization Considerations*

Design of a simple circular patch antenna (radius of $a$) is shown in Figure 1. The antenna consists of an infinitesimally thin metallic patch placed at a distance $h$ above a ground plane. The patch and the ground plane are separated by a dielectric substrate (relative permittivity of $\varepsilon_r$). A coaxial probe is used to feed the structure, where the inner conductor of the coaxial is attached to the radiating patch, while the outer conductor is attached to the ground plane. The resonance frequency of this antenna may be calculated as [10]

$$f_{\text{res}} = \frac{1.8412c}{2\pi a_e \sqrt{\varepsilon_r}}, \tag{1}$$

where $c$ is the speed of light in free-space and $a_e$ is the effective radius of the patch, which takes into account fringing according to

$$\alpha_e = \alpha\left\{1 + \frac{2h}{\pi\alpha\varepsilon_r}\left[\ln\left(\frac{\pi\alpha}{2h}\right) + 1.7726\right]\right\}^{1/2}. \tag{2}$$

Assuming the circular patch to be printed on a typical Rogers RO3210 substrate ($\varepsilon_r$ = 10.2, $h$ = 0.635 mm), which has long been used in implantable antenna design [9], [11], then its radius would have to approximately equal $a$ = 7.5 cm for operation in the MICS band ($f_{\text{res}}$ = 402 MHz).

Based on the above, miniaturization becomes one of the greatest challenges for implantable antenna design. Fortunately, human tissues in which implantable antennas are intended to operate exhibit high relative permittivity values ($\varepsilon_r$), which in turn work to advantageously reduce the physical size of the antenna. According to physics and electromagnetic (EM) theory, relative permittivity can be calculated as the real part of the complex relative permittivity

$$\varepsilon_c = \frac{\varepsilon}{\varepsilon_0} = \varepsilon_r - j\varepsilon_r \tan\delta, \tag{3}$$

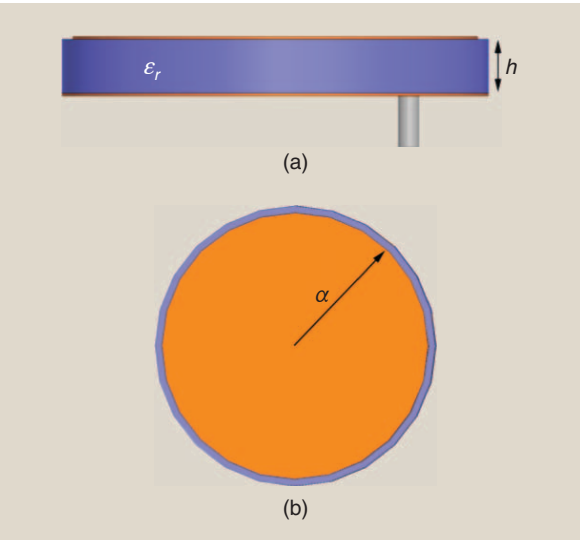


**Figure 1.** *The design of a simple circular patch antenna: (a) side and (b) face views.*

**TABLE 1. A size comparison of implantable patch antennas reported in the literature.**

| | | | Miniaturization Technique | | | | |
|---|---|---|---|---|---|---|---|
| **Ref.** | **Bands (MHz)** | **Implantation Tissue** | **Dielectric Material Permittivity** | **Patch Shape** | **Shorting Pin** | **Patch Stacking** | **Volume ($mm^3$)** |
| [12] | 402–405 | Skin | 10.2 | Spiral | No | No | 10,240.0 |
| [13] | 402–405 | 2/3 muscle | 2.94 | Waffle | Yes | No | 6,480.0 |
| [12] | 402–405 | Skin | 10.2 | Spiral | Yes | No | 6,144.0 |
| [8] | 402–405 | 2/3 muscle | 6.1 | Spiral | Yes | No | 3,457.4 |
| [14] | 402–405<br>2,400–2,800 | Skin | 6.1 | SRR coupled to spiral | Yes | No | 1,375.4 |
| [11] | 402–405<br>2,400–2,800 | Skin | 10.2 | Meandered | Yes | No | 1,265.6 |
| [15] | 402–405 | Skin | 10.2 | Spiral | Yes | No | 1,200.0 |
| [16] | 402–405 | Skin | 10.2 | Meandered | Yes | No | 1,200.0 |
| [17] | 402–405 | 2/3 muscle | 9.4 | Spiral | Yes | No | 823.0 |
| [18] | 402–405 | Muscle | 10.2 | $\pi$ Shaped | Yes | No | 790.9 |
| [19] | 402–405 | Mean body | 6.7 | Folded square | Yes | Yes | 448.0 |
| [20] | 402–405 | Skin | 10.2 | Hook-slotted | Yes | Yes | 335.8 |
| [21] | 402–405 | Vitreous humor | 10.2 | Spiral | Yes | Yes | 273.6 |
| [22] | 402–405<br>433–435<br>2,400–2,480 | Skin | 10.2 | Comb and $\pi$ shaped | Yes | Yes | 254.0 |
| [23] | 402–405 | Vitreous humor | 10.2 | Spiral | Yes | Yes | 254.0 |
| [9] | 402–405 | Skin | 10.2 | Meandered | Yes | Yes | 203.6 |
| [24] | 402–405 | Skin | 10.2 | Spiral | Yes | Yes | 190.0 |
| [25] | 402–405 | Skin | 10.2 | Hook slotted | Yes | Yes | 149.2 |
| [26] | 402–405 | Skin | 10.2 | Hook slotted | Yes | Yes | 121.6 |
| [27] | 402–405 | Skin | 10.2 | Meandered | Yes | Yes | 110.4 |
| [28] | 402–405 | Skin | 9.4 | Meandered | Yes | Yes | 32.7 |

where $\varepsilon_0$ is the free-space permittivity and $\tan\delta$ is the loss factor. For purely conductive losses

$$\tan\delta = \frac{\sigma}{\omega\varepsilon_0\varepsilon_r}, \tag{4}$$

where $\sigma$ is the medium conductivity.

The use of patch designs for implantable antennas allows for several additional miniaturization techniques, which can be summarized as follows [7].

- High-permittivity dielectric materials shorten the effective wavelength of the antenna, thus resulting in lower resonance frequencies.
- The effective current-flow path on the antenna's radiating patch can be increased through meandering or spiraling techniques.
- A shorting pin between the patch and ground planes acts somewhat like a ground plane on a monopole antenna, thus nearly doubling its size.
- Vertically stacking multiple radiating patches increases the length of the current-flow path, without significantly increasing the physical size of the antenna.

Table 1 compares the volume occupied by implantable patch antennas reported in the literature, with respect to the applied miniaturization techniques [8], [9],

[11]–[28]. The bands of operation covered and intended implantation tissue and are also included in Table 1. When the number of bands of operation is increased, the size of the antenna is typically increased to cover them. The performance of these antennas is further compared in Table 2 in terms of their 10-dB bandwidth (BW), maximum allowable input power levels imposed by the IEEE C95.1-1999 (1 g-avg SAR $\leq$ 1.6 W/kg [29]) ($P_{1999}$) and IEEE C95.1-2005 (10-g-avg SAR $\leq$ 2 W/kg [30]) ($P_{2005}$) safety guidelines, and maximum far-field gain ($G_{max}$).

**TABLE 2. A performance comparison of implantable patch antennas reported in the literature with respect to their occupied volume.**

| Ref. | Volume ($mm^3$) | BW (MHz) | $P_{1999}$ (mW) | $P_{2005}$ (mW) | $G_{max}$ (dBi) |
|---|---|---|---|---|---|
| [12] | 10,240 | 20 | 8.791 | N/A | N/A |
| [13] | 6,480 | 16 | N/A | N/A | N/A |
| [12] | 6,144 | 25 | 7.656 | N/A | N/A |
| [8] | 3,457.4 | 28 | N/A | N/A | N/A |
| [14] | 1,375.4 | 12 | N/A | N/A | –6 |
| [11] | 1,265.6 | 142 | N/A | N/A | –25 |
| [15] | 1,200 | 28 | 5.161 | N/A | N/A |
| [16] | 1,200 | 40 | 5.442 | N/A | N/A |
| [17] | 823 | 25 | 5.820 | N/A | N/A |
| [18] | 790.9 | 120 | 5.714 | N/A | –27 |
| [19] | 448 | 110 | 3.7 | N/A | N/A |
| [20] | 335.8 | 50 | 4.798 | N/A | –26 |
| [21] | 273.6 | 39 | N/A | N/A | –24 |
| [22] | 254 | 113 | 4.692 | N/A | –7 |
| [23] | 254 | 5 | N/A | 60.6 | –40 |
| [9] | 203.6 | 27 | 4.928 | 30.030 | –37 |
| [24] | 190 | 50 | 4.762 | N/A | –26 |
| [25] | 149.2 | 84 | 2.235 | N/A | yes |
| [26] | 121.6 | 122 | 1.778 | N/A | –38 |
| [27] | 110.4 | 50 | 1.932 | 20.704 | –46 |
| [28] | 32.7 | 40 | 2.354 | 24.390 | –45 |

NOTE: N/A denotes that this information is not available.

## Biocompatibility Considerations

Implantable antennas must be biocompatible in order to preserve patient safety and prevent rejection of the implant. Furthermore, human tissues are conductive and will short-circuit the implantable antenna if they are allowed to be in direct contact with its metallization. In the literature, there have been reported two approaches for preserving the biocompatibility of implantable antennas and separating their metallic parts from the surrounding biological tissues: 1) covering the antenna structure with a biocompatible superstrate dielectric layer (e.g., Teflon, MACOR, ceramic alumina [8]) and 2) insulating the antenna with a thin layer of low-loss biocompatible coating (e.g., Zirconia [29], poly-ether-ether-ketone (PEEK) [32], Silastic Grade Elastomer [33]) [34].

## Prototype Fabrication Considerations

Fabrication of implantable antenna prototypes introduces some additional considerations that need to be taken into account within the numerical design stage. Due to the miniature size of these structures, inconsistencies between the numerical antenna model and fabricated prototype related to the following considerations, might result in a nonfunctional prototype [7], [32].

- **Gluing.** Glue layers are to be inserted between multiple substrate layers and/or between substrate and superstrate layers of the antenna for bonding purposes.
- **Metallization.** Even though zero-thickness and perfectly conducting sheets are usually used to model the radiating and ground planes of a patch antenna, the fabricated prototype is expected to exhibit finite-thickness conductive sheets made of copper material.
- **Feeding.** Ideal models of 50-Ω coaxial cables are usually used to feed the numerical antenna models. However, it is highly recommended to carry out simulations for implantable antennas while considering the actual dimensions and material properties of the commercial coaxial cable to be used in fabrication.

It is important to emphasize that metallization and feeding parameters might often be ignored within the numerical design of implantable antennas for simplification and acceleration purposes. On the contrary, gluing has been found to be a very critical fabrication-related factor for implantable antenna design and has to be taken into account: low-permittivity glue layers isolate the high-permittivity substrate layers, thus decreasing the effective permittivity and electrical length of the antenna while increasing its resonance frequency [35].

## Proposed Parametric Implantable Antenna Model

The parametric implantable antenna model of Figure 2 is proposed to serve the goals of this tutorial. The antenna model addresses all aforementioned considerations related to miniaturization, biocompatibility, and prototype fabrication [9], [35], [36]. The model consists of a ground plane (radius of $R$) and two vertically stacked patches (radius of $R - 0.1$ mm each), printed

on dielectric substrates (permittivity of $\varepsilon_{rd}$ and thicknesses of $h_1$ and $h_2$, respectively). The origin of the coordinate system is considered to be located at the center of the antenna ground plane. A dielectric superstrate (permittivity of $\varepsilon_{rd}$ and thickness of $h_3$) covers the structure for biocompatibility purposes. Meanders of variable lengths ($L_i$, $i$ = 1–5, 1′–6′) and identical widths (0.4 mm) are inserted into the patches to assist in miniaturization. A shorting pin ($S$:($s_x$,$s_y$)) connects the ground plane to the lower patch, while a 50-Ω coaxial cable of variable type and length ($L$) excites both patches ($F$:($f_x$,$f_y$)). Copper sheets (thickness of $h_m$) are considered for the ground plane and patches, while glue layers (permittivity of $\varepsilon_{rg}$ and thickness of $h_g$) bond the dielectric layers together.

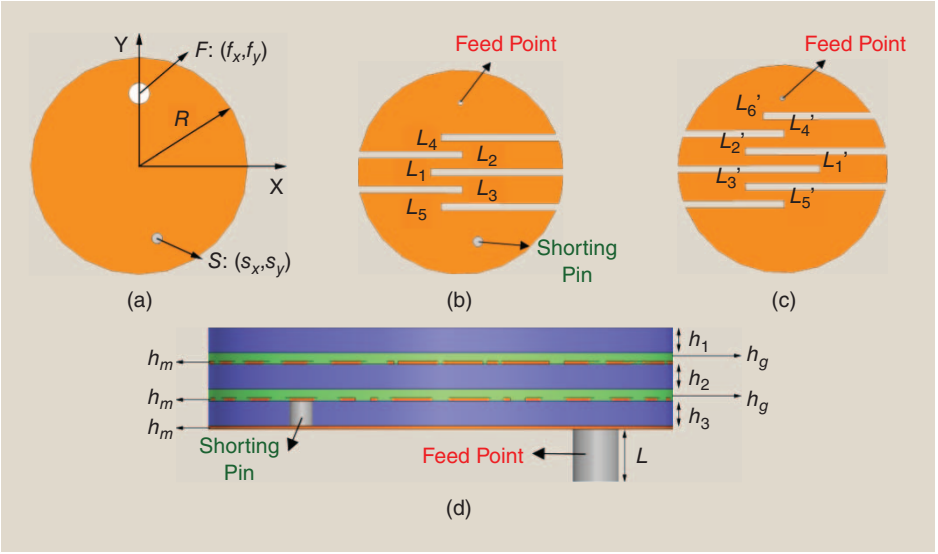


**Figure 2.** *The proposed parametric implantable antenna model: (a) ground plane, (b) lower patch, (c) upper patch, and (d) side view.*

## Numerical Design and Performance Evaluation of the Implantable Antenna

### *Numerical Design*

Once the parametric implantable antenna model has been selected, the next step is to appropriately tune its design parameters using an EM modeling and simulation program. The goal is to quickly calculate those parameter values that will optimize antenna design in terms of impedance matching as well as exhibited radiation and patient safety performance at the desired operating frequency. The flow chart of the suggested methodology is shown in Figure 3 [37] and is further applied within the framework of tuning the parametric implantable antenna model of Figure 2 for ICP monitoring [38] at 402 MHz (MICS band) [9], [35].

#### Fabrication-Related Parameters

Initially, fabrication-related parameters of the antenna are set to the values dictated by the intended fabrication procedure (Table 3). As part of this tutorial, Rogers RO3210 ($\varepsilon_{rd}$ = 10.2) dielectric sheets with a thickness of 0.635 mm ($h_1 = h_2 = h_3 = 0.635$ mm) are considered because of their availability in our lab and their similarity in electrical properties to those of biocompatible ceramic alumina [39]. The aforementioned dielectric sheets come premetalized with a 0.017-mm-thick electrodeposited copper foil ($h_m$ = 0.017 mm). Sprayable glue 3M 77 is used to bond the layers ($\varepsilon_{rg}$ = 2.0), which has been found to exhibit an average thickness of 0.3 mm ($h_g$ = 0.3 mm) for the fabrication process to be followed. The antenna is to be fed by means of a 50-mm-long ($L$ = 50 mm) EZ-47 (center conductor diameter of 0.29 mm, polytetrafluoroethylene (PTFE) dielectric with a diameter of 0.93 mm, outer conductor diameter of 1.19 mm) semirigid coaxial cable.

#### Size-Related Parameters

The size-related parameters of the antenna have to be selected, i.e., the parameters that determine the outer dimensions (physical size) of the antenna. In the parametric implantable antenna model considered in this tutorial, these are dictated by the antenna radius, $R$. Selection of the outer dimensions relies on the expertise and knowledge of the designer and must be performed based on the following two considerations. First, size of the implantable antenna needs to take into account the desired implantation site and medical application scenario as well as the size of the IMD in which it will be integrated. Second, miniaturization should not be set as the sole goal of the design. Previous studies have demonstrated degraded radiation and patient safety performance with size reduction for implantable antennas and have quantified this degradation as a function of size [40]. Given these considerations, a radius of $R$ = 6 mm is selected for the ICP monitoring antenna under study (Table 3).

#### "To-Be-Optimized" Parameters

The rest of the design parameters are considered as dimensions in the solution space and have to be tuned for an optimized 50-Ω impedance match at the desired operating frequency (to-be-optimized). Design is performed by setting the fabrication-related and size-related parameters to the values selected

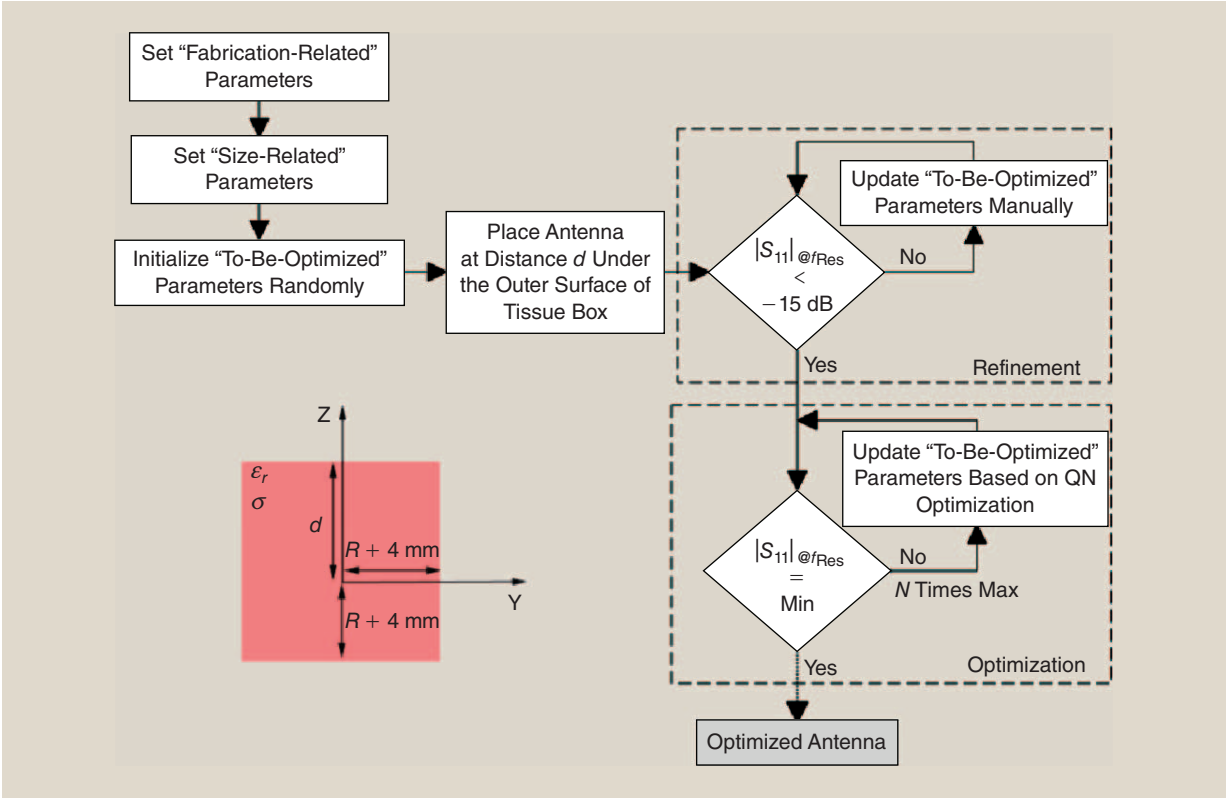


**Figure 3.** *A flow chart of the proposed methodology for numerical design of implantable antennas.*

in the previous steps, initializing the to-be-optimized parameters to random values and placing the antenna at a distance $d$ under the outer surface of the tissue-simulating box shown in the inset of Figure 3 [37]. The distance $d$ corresponds to the actual air-to-antenna separation distance for the desired medical application scenario (implantation depth). The tissue-simulating box extends by ($R$ + 4 mm) in the $x$ and $y$ directions ($R$ is the maximum dimension of the antenna in the positive $y$ axis) and simulates the electrical properties of the intended implantation tissue ($\varepsilon_r$,$\sigma$) [41]. These can be either approximated as constant within a narrow frequency range [9], [28] or described by means of a Cole-Cole formulation for the complex relative permittivity, according to

$$\varepsilon_c(\omega) = \varepsilon_\infty + \sum_n \frac{\Delta\varepsilon_n}{1 + (j\omega\tau_n)^{(1-\alpha_n)}} + \frac{\sigma_i}{j\omega\varepsilon_0}, \tag{5}$$

where $\omega$ is the angular frequency, $n$ is the order of the Cole-Cole model, $\varepsilon_\infty$ is the high frequency permittivity, $\tau_n$ is the relaxation time, $\Delta\varepsilon_n$ is the pole amplitude, $\alpha_n$ is the parameter that allows for the broadening of the dispersion, and $\sigma_i$ is the static ionic conductivity [42], [43]. Radiation boundaries have to be set at a distance of $\lambda_0/4$ away from the tissue-simulating box to extend radiation infinitely far and guarantee stability of the numerical simulations ($\lambda_0$ is the free-space wavelength at $f_{res}$).

In the refinement step, an approximate design is performed for the antenna. The to-be-optimized parameters are manually updated in an iterative way, until the magnitude of the reflection coefficient ($|S_{11}|$) at the desired operating frequency (fres) satisfies

$$|S_{11}|_{@fres} <- 15 \text{ dB}. \tag{6}$$

A manual update relies on the skills and expertise of the designer, who is considered to be aware of the theoretical background related to antenna miniaturization (e.g., longer meanders are expected to increase the length of the current flow and result in lower resonance frequencies [44], [45], etc.).

In the optimization step, antenna design is optimized. The to-be-optimized parameters are initialized to the values of the refinement step and are optimized based on a software-integrated optimization algorithm. The optimization process terminates when

$$|S_{11}|_{@fres} = \min \tag{7}$$

or when the number of iteration exceeds a predefined maximum number.

As part of this tutorial, the finite element-based Ansoft high-frequency structure simulator (HFSS) software is used [46]. Simulations are performed at a distance of $d = 5$ mm under the outer surface of a small ($R = 6$ mm) tissue-simulating box, which corresponds

**TABLE 3. Parameter values selected for optimally tuning the implantable antenna model of Figure 2 at 402 MHz (MICS band).**

| | Parameters | Values |
|---|---|---|
| Fabrication related | $\varepsilon_{rd}$ | 10.2 |
| | $\varepsilon_{rg}$ | 2.0 |
| | $h_1$ | 0.635 mm |
| | $h_2$ | 0.635 mm |
| | $h_3$ | 0.635 mm |
| | $h_m$ | 0.017 mm |
| | $h_g$ | 0.3 mm |
| | $L$ | 50 mm |
| | Coaxial type | EZ–47 |
| Size related | $R$ | 6 mm |
| To be optimized | $L_1$ | 7.597 mm |
| | $L_2$ | 10.146 mm |
| | $L_3$ | 10.146 mm |
| | $L_4$ | 3.019 mm |
| | $L_5$ | 3.019 mm |
| | $L_{1'}$ | 11.397 mm |
| | $L_{2'}$ | 11.146 mm |
| | $L_{3'}$ | 11.146 mm |
| | $L_{4'}$ | 10.519 mm |
| | $L_{5'}$ | 10.519 mm |
| | $L_{6'}$ | 8.993 mm |
| | $s_x$ | 1 mm |
| | $s_y$ | −4 mm |
| | $f_x$ | 0 mm |
| | $f_y$ | 4 mm |

to the actual average implantation depth of an ICP monitor inside the human scalp. The tissue-simulating box represents skin-tissue (scalp) electrical properties at $f_{res}$ = 402 MHz ($\varepsilon_r$ = 46.7, $\sigma$ = 0.69 S/m [41]), which are approximated as constant inside the 300–500 MHz range. Using this approximation, the maximum errors of $\varepsilon_r$ and $\sigma$ are given by 6.59% and 8.89%, respectively. The to-be-optimized parameters of the antenna are optimized based on quasi-Newton optimization (the maximum number of iterations is set to 300), due to its

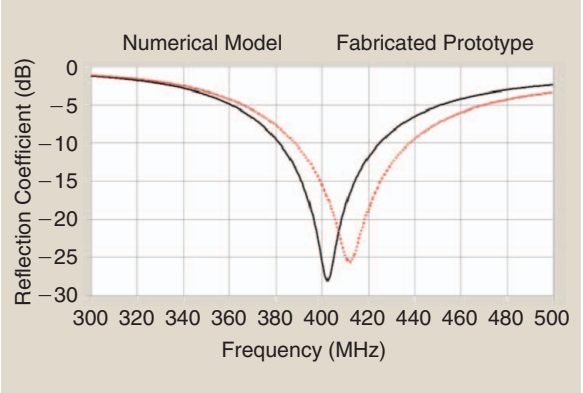


**Figure 4.** *Numerical and in vitro measured reflection coefficient frequency response of the proposed implantable antenna for ICP monitoring.*

speed and accuracy in cases of insignificant numerical noise [47]. Optimal parameter values are given in Table 3, whereas the reflection coefficient frequency response of the designed antenna is shown in Figure 4 (numerical model). The antenna resonates at 402 MHz with a reflection coefficient of −27.9 dB, and a wide 10-dB BW of 44 MHz, which covers the MICS band.

It is worth noting that a few other methodologies have also been reported in the literature for implantable antenna design [9], [32], [37]. However, the aforementioned methodology has been shown to result in the fastest design of implantable antennas with optimized resonance characteristics within the medical band in hand. The reason is that it incorporates dielectric loading of both the surrounding tissues and exterior air on the antenna while employing a canonical (parallelepiped) miniature tissue model, which can be meshed and solved in a relatively easy and fast way [37]. Equivalently, the tissue-simulating box considered in this methodology has been found to be the simplest and smallest tissue model in which the implantable antenna exhibits almost identical reflection coefficient frequency response as it would exhibit inside a canonical or anatomical tissue model of the intended implantation site [37].

### *Performance Evaluation*

If desired, the designed antenna model can further be placed inside a canonical or anatomical model of the intended implantation site and evaluated in terms of the exhibited resonance, radiation, and safety performance.

As part of this tutorial, the parameters of the implantable antenna model (Figure 2) are set to those of Table 3, and the antenna is placed at a distance of 5 mm under the skin of a 13-tissue anatomical head model [Figure 5(a)] [35]. Tissue electrical properties at 402 MHz [41] are considered to simulate an ICP monitoring scenario in the MICS band. Simulations are carried out in Remcom X finite difference time domain

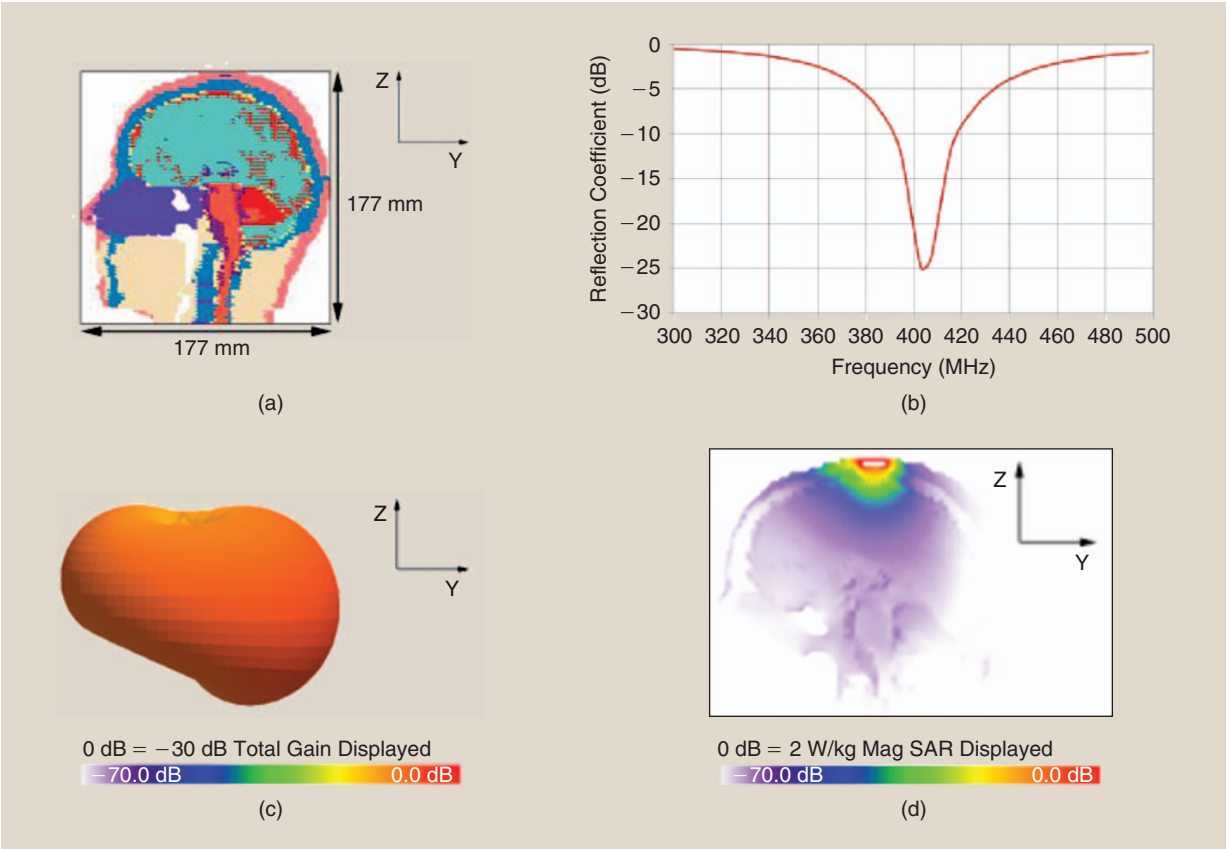


**Figure 5.** *Performance evaluation of the proposed implantable antenna for ICP monitoring: (a) 13-tissue anatomical head model, (b) reflection coefficient frequency response, (c) far-field gain radiation pattern, and (d) local SAR distribution for the ZY slice where maximum local SAR has been recorded (net-input power of 4.927 mW).*

(XFDTD) [48], which applies the finite-difference, time domain method to efficiently model and solve detailed anatomical body parts. The reflection coefficient frequency response of the antenna is shown in Figure 5(b), and, as expected, it is almost identical to that of Figure 4 (numerical model). The antenna inside the anatomical head model radiates an asymmetrical far-field gain radiation pattern [Figure 5(c)] with a maximum gain of –37.10 dBi. Low gain is attributed to the small antenna size and high tissue loss. Maximum 1 g-averaged (1 g-avg) and 10 g-averaged (10 g-avg) specific absorption rate (SAR) values equal 324.74 and 65.09 W/kg, respectively, for a net input power of 1 W. Therefore, the IEEE C95.1-1999 [29] and IEEE C95.1-2005 [30] safety standards limit the maximum allowable net-input power to the antenna to 4.927 and 30.73 mW, respectively. Local SAR distribution is shown in Figure 5(d) for a net-input power of 4.927 mW, considering the ZY slice where maximum local SAR has been recorded.

## Fabrication of the Implantable Antenna Prototype

Fabrication of implantable antenna prototypes needs to deal with all challenges related to the fabrication of miniature antenna structures and is, therefore, highly intriguing. After a number of preliminary tests for establishing and optimizing the best fabrication approach, the latter is hereafter presented within the framework of fabricating the implantable ICP monitoring antenna under study (i.e., the parametric implantable antenna model of Figure 2 with its parameter values set to those of Table 3).

Three key aspects of the fabrication are considered to mainly influence the final antenna behavior: 1) substrate cutting, 2) substrate gluing, and 3) layer alignment. One of the problems is that these three steps are not necessarily independent. In fact, because the substrate material is relatively stiff, it cannot (or is hard to) be cut after the antenna has been assembled; microsoldering of the coaxial cable and shorting pin are very fragile and cannot withstand the vertical pressure and torsion of the cutting tool. Furthermore, external alignment points are proved to be required for the assembling, to be removed after fabrication. Therefore, a mounting base [Figure 6(a)] is suggested to be fabricated in order to help in the antenna's assembly. This base ensures the correct alignment between the three layers while serving as the antenna support for the different soldering procedures.

Based on the above, the proposed fabrication methodology includes the following steps.

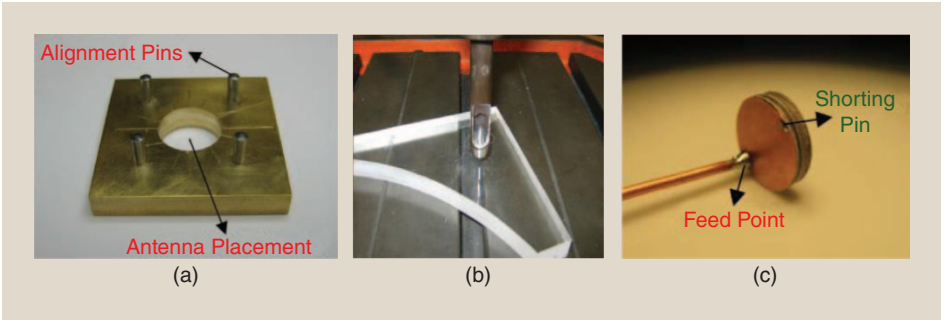


**Figure 6.** *Fabrication methodology under consideration: (a) mounting base, (b) circular cutting tool, and (c) fabricated prototype of the proposed implantable antenna for ICP monitoring [35].*

- **Photolithography masks.** Photolithography masks are prepared and printed, as shown in Figure 7. The masks include: 1) a circular circumference, which is used to guide the antenna cutting, 2) four circular marks, which indicate the position of the holes that match the four pins of the mounting base [Figure 6(a)] during the assembly procedure, 3) a square frame, which matches the dimensions of the mounting base [Figure 6(a)], and 4) complementary alignment marks to help in the alignment of the two sides of the bottom substrate layer (i.e., ground plane and lower patch).
- **Photolithography.** The acquired Rogers RO3210 dielectric layers ($\varepsilon_{rd} = 10.2, h_1 = h_2 = h_3 = 0.635$mm, $h_m = 0.017$ mm) are etched by means of a photolithographic process, which makes use of the photolithography masks of the previous step. The lower substrate layer contains the ground plane and the lower patch, the upper substrate contains the upper patch, while the superstrate has no metallization.
- **Cutting of the layers.** A circular cutting tool is used to cut the antenna layers, as shown in Figure 6(b). The cutting tool exhibits a nominal diameter of 12 mm, which corresponds to the diameter of the intended antenna prototype ($R = 6$ mm). The adopted strategy is to precut the substrate down to a critical depth, just enough to keep the alignment points together with the patch, but weak enough to allow easy detaching without much mechanical stress to the antenna.
- **Antenna assembly.** The antenna is further assembled by making use of the mounting base of Figure 6(a). Layers are aligned and glued (3M 77 glue: $\varepsilon_{rg} = 2.0$, $h_g = 0.3$ mm), while the shorting pin is set to connect the ground plane to the lower patch through a via. The outer conductor of the EZ-47 coaxial cable gets connected to the antenna ground plane while the inner conductor gets simultaneously soldered to the lower and upper patches through vias. Nevertheless, detaching the antenna from the excess alignment material has been shown to be relatively hard, thus resulting in some stress to the fragile antenna.

It is worth noting that several details of the fabrication procedure under consideration have already been taken into account within the numerical design step, where they provided input for selecting the fabrication-related parameters of the antenna. The assembled antenna is shown in Figure 6(c). The most critical aspect regarding the fabrication of such miniature implantable antennas is the control of the glue layer thickness. This is impaired not only by the glue itself but also by the slight bump of the microsolder near the coaxial cable and the shorting pin that prevents perfect contact between the layers.

## In Vitro Testing of the Implantable Antenna Prototype

### *Phantom Setup Selection and Sensitivity Tests*

The first step before proceeding with in vitro testing of an implantable antenna prototype is to decide on the phantom setup, i.e., the geometry of the phantom to be used, and the relative positioning of the antenna

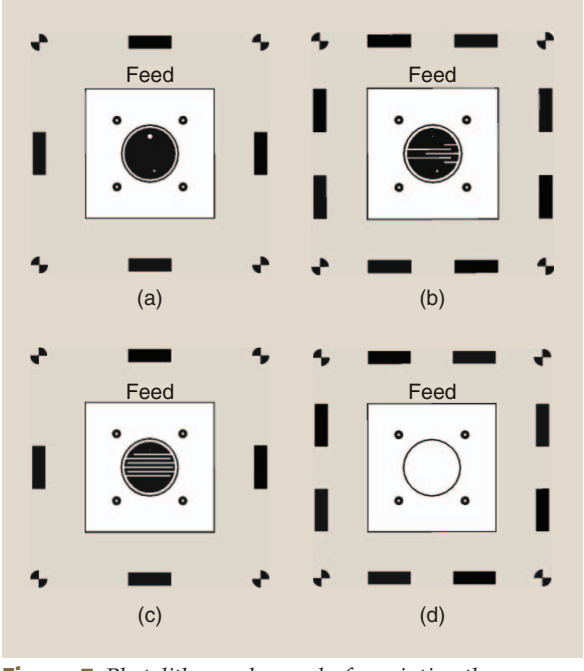


**Figure 7.** *Photolithography masks for printing the proposed implantable antenna for ICP monitoring: (a) ground plane, (b) lower patch, (c) upper patch, and (d) superstrate.*

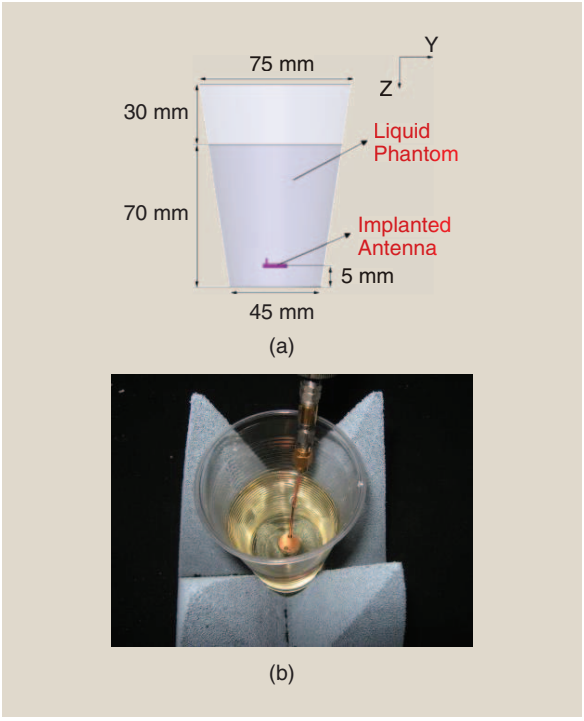


**Figure 8.** *In vitro testing of the proposed implantable antenna for ICP monitoring: (a) numerical model and (b) experimental setup [35].*

inside it. As highlighted in the "Numerical Design and Performance Evaluation of the Implantable Antenna" section, design of the implantable antenna allows for the selection of any phantom, as long as the antenna is placed at a distance $d$ under its outer surface (inset of Figure 3) and is surrounded by the same tissue material as the one in which numerical design took place.

Numerical tests should further be performed with the designed antenna placed inside a numerical model of the selected phantom, aiming to assess tolerance to the most sensitive experimental factors. At this step, theoretical electrical properties may be assumed for the phantom, which should match those of the tissue-simulating box in which numerical design took place (Figure 3). The goal is to calculate the expected range of uncertainty in experimental results, or, equivalently, the maximum allowable deviation between numerical and experimental results. If results of the subsequent in vitro testing lie within the acceptable uncertainty limits, then fabrication and testing of the implantable antenna under consideration can be considered as successful.

As part of this tutorial, we consider the designed ICP monitoring antenna to be placed 5 mm under the outer surface of a typical plastic drinking glass semifilled with skin tissue-emulating liquid at 402 MHz ($\varepsilon_{\text{rph}} = 46.7, \sigma_{\text{ph}} = 0.69$ s/m[41]) [Figure 8(a)]. Sensitivity test results are indicated in Figure 9. Only the antenna or phantom parameter under investigation is considered variable in each case, while all other parameters are kept constant and equal to those of the original setup. The exhibited resonance frequency ($f_{\text{res}}$) and reflection coefficient at this frequency ($|S_{11@\text{fres}}|$) is recorded in each case, while resonance performance of the original setup is also indicated for reference. Given the fabrication approach described in the "Fabrication of the Implantable Antenna Prototype" section, the following sources of potential experimental uncertainties are identified and examined [35].

- **Gluing** ($\varepsilon_{\text{rg}}, h_g$) [Figure 9(a)]. Air bubbles accumulating within the glue prevent $\varepsilon_{\text{rg}}$ from being accurately determined. Furthermore, the adopted layer bonding process does not allow fine control of $h_g$. This is impaired not only by the glue itself but also by the slight bump of the microsolder near the coaxial cable and the shorting pin that prevents perfect contact between the layers. Deviations of $\pm 10\%$ and 33% in $\varepsilon_{\text{rg}}$ and $h_g$ are found to cause frequency detunings by up to 1.7% and 6.2%, respectively.
- **Antenna radius** ($R$) [Figure 9(b)]. Rogers RO3210 requires significant mechanical stress (vertical pressure and torsion) for detaching the excess alignment material, thus degrading accuracy of the cutting procedure. A 0.2-mm increase in $R$ detunes the antenna by 4.4%, whereas a 0.1-mm decrease brings the copper patch sheets in direct contact with the tissue, thus significantly degrading the resonance performance of the antenna.
- **Relative rotation between the patches** (indicated by the rotation of the lower $\varphi_l$ and upper $\varphi_u$ patches around the z-axis) [Figure 9(c)]. Even though alignment marks are included in the photolithography masks, the alignment setup is relatively relaxed with respect to angular misalignment of the layers. Misalignment by 10° is found to cause a maximum frequency detuning of only 1.2%, thus proving to be of minor importance. Positive and negative rotation angles correspond to clockwise and counterclockwise rotation around the z-axis, respectively.
- **Permittivity of the Rogers RO3210 dielectric material** ($\varepsilon_{\text{rd}}$) [Figure 9(d)]. The typical value of the Rogers RO3210 permittivity is defined to be 10.2 at 10 GHz under 23 °C. However, frequency and temperature variations may slightly affect ($\varepsilon_{\text{rd}}$) and degrade antenna performance. Nevertheless, sensitivity tests indicate minor effects in the exhibited resonance performance; variations of $\pm 0.4$ in $\varepsilon_{\text{rd}}$ may lead to frequency detunings by up to only 1%.
- **Electrical properties of the phantom** ($\varepsilon_{\text{rph}}, \sigma_{\text{ph}}$) [Figure 9(e)]. Permittivity and conductivity values of the phantom might not exactly match the theoretical ones, whereas time and room temperature

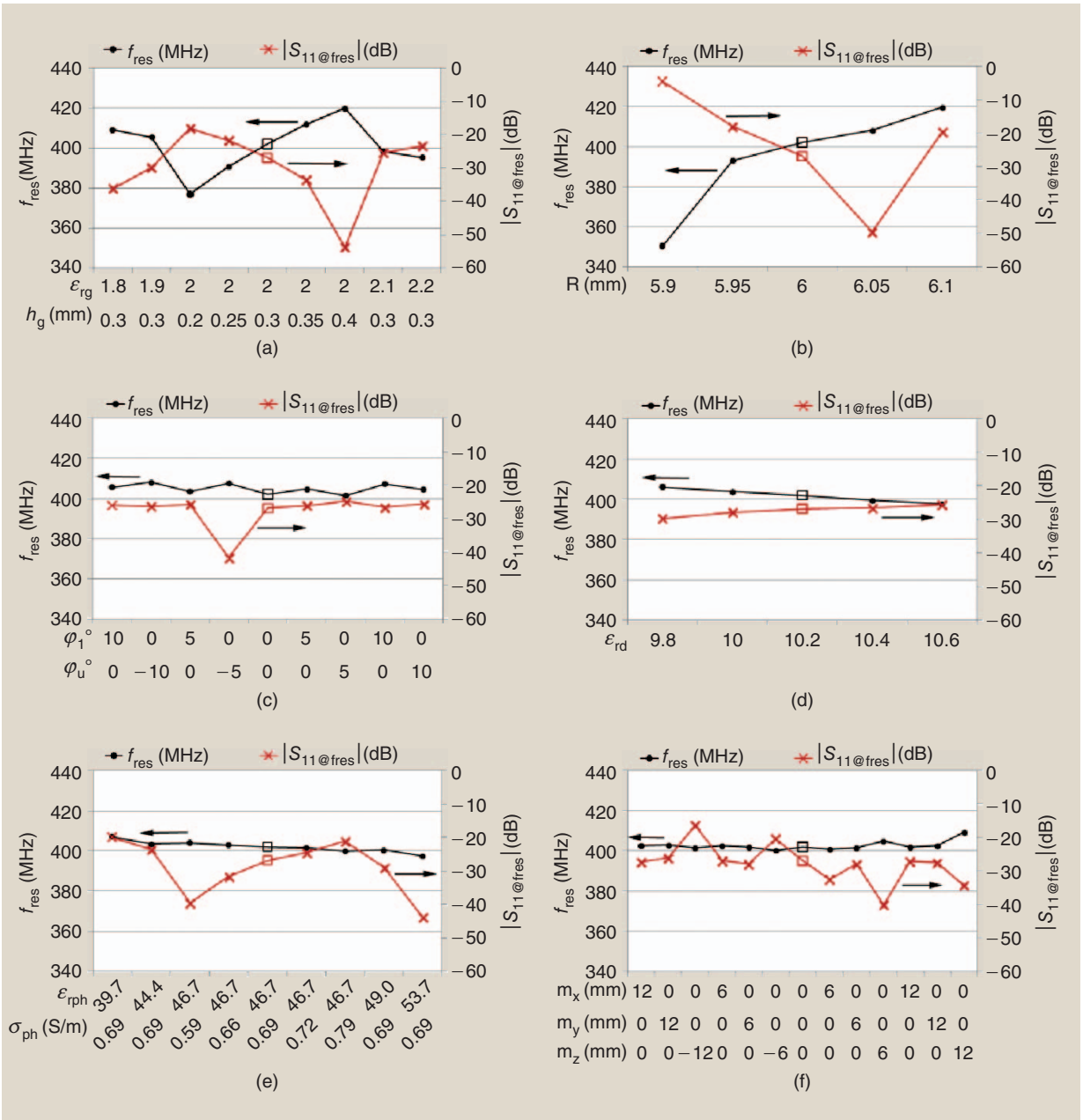


**Figure 9.** *Sensitivity test results related to the following parameters: (a) gluing ($\varepsilon_{rg}$,$h_g$), (b) antenna radius (R), (c) relative rotation between the patches ($\varphi_l$,$\varphi_u$), (d) permittivity of the Rogers RO3210 dielectric material ($\varepsilon_{rd}$), (e) electrical properties of the phantom ($\varepsilon_{rph}$,$\sigma_{ph}$), and (f) relative antenna-phantom position ($m_x$, $m_y$, $m_z$) [35].*

may further perturb these properties from their nominal values. Changes in $\varepsilon_{rph}$ and $\sigma_{ph}$ by 15% are found to degrade antenna resonance by up to 1.2% and 0.5%, respectively.

- **Relative antenna-phantom position** [indicated by the relative shift of the phantom ($m_x$,$m_y$,$m_z$) from its original position] [Figure 9(f)]. Since the antenna is manually positioned inside the phantom, slight deviations from the immersion scenario of Figure 8(a) may occur. As expected, numerical results indicate insensitivity to antenna positioning inside the phantom as long as it is surrounded by skin-tissue.

### *In Vitro Testing*

In vitro testing of implantable antennas involves measurement of their reflection coefficient frequency response while immersed inside phantoms, which emulate the intended implantation scenario. This involves the following three steps.

- **Phantom formulation.** In the literature, several recipes for emulation of biological tissues at various frequencies, including the MICS band (e.g., [11], [49], [50]), have been presented. Gels rather than liquids are preferred in cases where multilayer phantoms and, thus, increased realism in experimental modeling, are solicited. Deionized

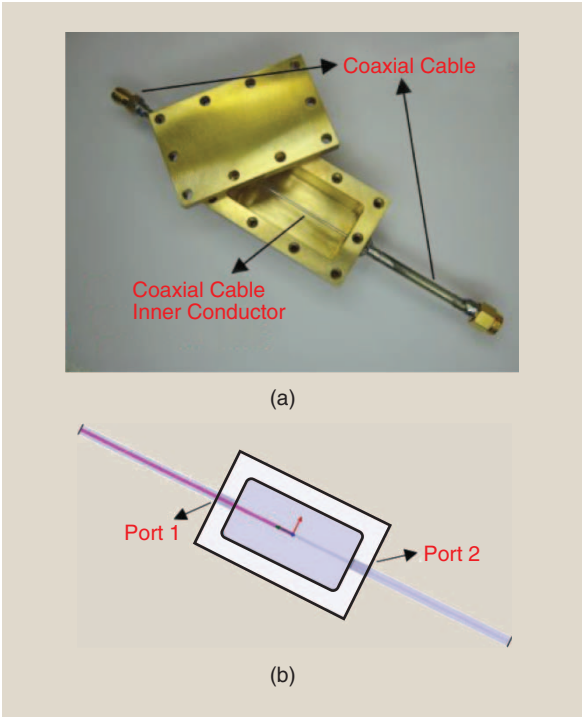


**Figure 10.** *A complex permittivity measurement of liquid and semisolid phantoms: (a) coaxial container and (b) numerical model [35].*

or distilled water usually acts as the base ingredient of the phantoms. The addition of sugar or glycerol reduces permittivity ($\varepsilon_{rph}$), almost without affecting conductivity ($\sigma_{ph}$). Salt increases $\sigma_{ph}$ and slightly increases $\varepsilon_{rph}$ [11]. Solidification is usually made possible with agar. Other ingredients may also be used in order to vary the viscosity, preserve the mixture, and further control $\varepsilon_{rph}$ and $\sigma_{ph}$ [49], [50]. As part of this tutorial, a liquid is formulated from deionized water (41.48%), sugar (56.18%), and salt (2.33%), which emulates skin-tissue properties at 402 MHz ($\varepsilon_{rph} = 46.7$, $\sigma_{ph} = 0.69$ S/m) [11].

- **Measurement of the phantom electrical properties.** In vitro testing of implantable antennas inside phantoms requires experimental measurement of the exhibited electrical properties ($\varepsilon_{rph}, \sigma_{ph}$) to ensure conformance with the corresponding theoretical values. Recently, an in-depth analysis has been provided for the measurement of the electrical properties of biological media [51]. In the market, there exist some commercial complex permittivity measurement systems, such as the Agilent Technologies 85071E (Agilent Technologies, Santa Clara, California, United States), or the SPEAG Dielectric Assessment Kit (SPEAG, Switzerland). However, alternative approaches are further solicited for laboratories that are not equipped with such commercial systems. For example, a low-cost and reliable complex permittivity measurement technique has recently been proposed [35]. The measurement setup consists of a parallele-piped container intercepted by the inner conductor of a coaxial cable, as shown in Figure 10(a) (exterior container size of 52 mm $\times$ 32 mm $\times$ 32.2 mm, interior cavity size of 40 mm $\times$ 20 mm $\times$ 20 mm). The coaxial container is filled with the liquid or gel dielectric material under investigation, and once the lid is closed, it represents a transition between coaxial guides with a step characteristic impedance discontinuity. The transfer function between the two coaxial connectors outside the container depends upon the complex permittivity of the container's filling material. This can be de-embedded by comparing the measured scattering-matrix (S-matrix) with simulation results for the same structure [Figure 10(b)]. As part of this tutorial, the aforementioned cavity is filled with the skin-emulating liquid formulated in the previous step. Experimental results are shown in Figure 11. These are superimposed with numerical results for the cavity filled with a dielectric material which simulates skin-tissue properties at 402 MHz ($\varepsilon_{rph} = 46.7$, $\sigma_{ph} = 0.69$ S/m). Quite good agreement is observed at 402 MHz, indicating the adequacy of the formulated mixture for in vitro testing of the MICS implantable antenna under study.
- **In vitro measurement of the implantable antenna.** The phantom geometry selected in the section "Phantom Setup Selection and Sensitivity Tests" is subsequently filled with the formulated liquid or gel dielectric material. The implantable antenna prototype is connected to a network analyzer and immersed inside the phantom at a distance $d$ from its outer surface. The exhibited reflection coefficient frequency response is then measured and compared to numerical results for the same structure (see the "Numerical Designs" section), by taking into account the corresponding sensitivity tests results. Care must be taken within measurements regarding the presence of the coaxial cable, which is used for testing purposes. Nevertheless, it has been shown that the coaxial cable has a minor effect on implantable patch antennas whose ground planes are in direct contact with the phantom; high losses of the equivalent biological medium attenuate the currents on the back side of the ground plane, thus preventing their flow on the cable [52]. As part of this tutorial, the implantable antenna prototype of Figure 6(c) is placed at a distance of 5 mm from the outer surface of the phantom selected in the "Phantom Setup Selection and Sensitivity Tests" section [Figure 8(a)], and connected to an Agilent network analyzer (Agilent Technologies,

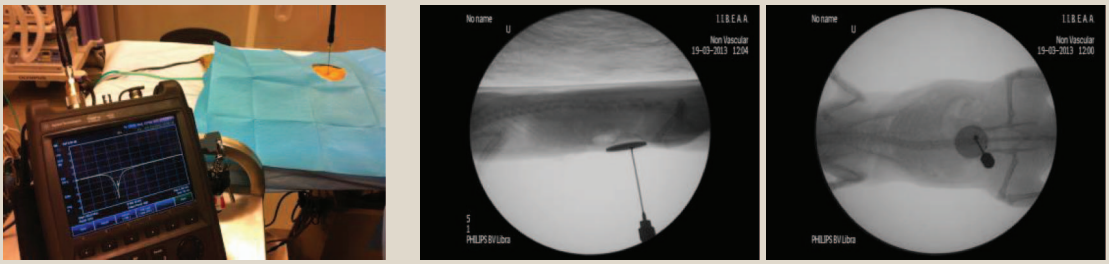


**Figure 11.** *In vivo testing of the proposed implantable antenna for ICP monitoring: (a) experimental setup and (b) X-ray images obtained through fluoroscopy.*

Santa Clara, California). The experimental setup is shown in Figure 8(b), whereas the measured reflection coefficient frequency response is superimposed in Figure 4 (prototype). Good agreement exists between numerical and experimental results. A slight resonance shift of 10 MHz (2.5%) is observed, which lies within the uncertainty allowances imposed by the sensitivity tests. Both simulation and measurement exhibit a 10-dB BW, which includes the MICS band.

## In Vivo Testing of the Implantable Antenna Prototype

In vitro verification of an implantable antenna does not guarantee its proper functioning when implanted inside actual biological tissues [33]. Therefore, once functionality of an implantable antenna prototype has been verified in vitro, in vivo testing is recommended. This includes implantation of the fabricated prototype inside model animals and subsequent measurement of the exhibited reflection coefficient frequency response. The goal is to compare the numerical and in vivo experimental results in an attempt to assess the effects of the following factors which affect in vivo experimentation:

- air gaps between the implanted antenna and the surrounding tissues
- presence of multiple types of tissues around the antenna
- dependence of tissue electrical properties upon frequency
- intersubject variability (anatomy and dependence of tissue electrical properties upon each rat's age, size, sex, internal body temperature, etc.)
- variations in the surgical procedures followed (implantation depth, implantation site, length of the wound, closure of the wound with sutures, etc.).

The first step in in vivo experimentation is the development of an experimental measurement protocol. The protocol has to be developed in cooperation with an experimental surgery unit; take into account legal requirements regarding the care and use of laboratory animals; and address issues related to the type and number of model animals, implantation site of the antenna, anesthesia, surgical procedure, measurements, and postsurgery treatment.

As part of this tutorial, the fabricated implantable antenna prototype of Figure 6(c) (radius of $R$) is tested in vivo. Experimentation is based on an in vivo protocol, which has been developed in cooperation with the Center for Experimental Surgery of the Biomedical Research Foundation Academy of Athens (CES–BRFAA), takes into account the legal requirements regarding the care and use of laboratory animals in Greece and can be summarized as follows [53]

- **Type and number of model animals.** Implantation and measurements are carried out inside rats, which have long been used in the literature as model animals [33]. Wistar outbred rats (HsdOla:WI) are employed, which exhibit a mean and standard deviation (SD) body weight of 331.3 ± 9.2 g. In order to assess inter-subject and surgical procedure variability, each antenna is implanted and measured inside three different rats.
- **Implantation site of the antenna.** Since the antennas under study have been designed for operation inside soft tissues, implantation is carried out within the subcutaneous tissue of the rats' abdomen.
- **Anesthesia.** Each rat is first anesthetized with an intraperitoneal (i.p.) injection of 70 mg/kg ketamine (Ketaset, Fort Dodge, Iowa) and 5 mg/kg xylazine (Rompun, Bayer, Leverkusen, Germany).
- **Surgical procedure.** A wound with a length of $(2{\cdot}R + 5$ mm) is further made in the rat's abdomen area, and the antenna is implanted within the abdominal subcutaneous tissue ($2{\cdot}R$ is the maximum physical size of the antenna). Following implantation, the wound is closed with 0/4 silk sutures (Silkam, Braun, Aesculap, Tuttlingen, Germany), leaving a 2-mm opening for the feeding coaxial cable to exit the skin.
- **Measurements.** Right after surgery, the feeding coaxial cable is connected to an Agilent Fieldfox

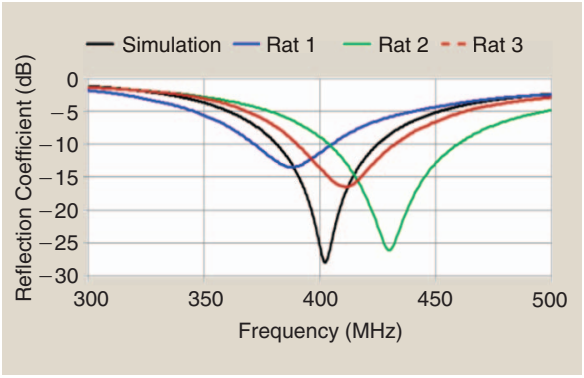


**Figure 12.** *Numerical and in vivo measured reflection coefficient frequency responses of the proposed implantable antenna for ICP monitoring.*

handheld network analyzer (Agilent Technologies, Santa Clara, California). The reflection coefficient frequency response exhibited by the antenna under study is further recorded and saved. Measurement is carried out within the 300–500 MHz frequency range, which symmetrically covers the MICS band.

- **Post-surgery treatment.** Once measurement is completed, the implanted antenna is removed, and the rat is euthanized in a $CO_2$ chamber. Time lapse from the start of the surgical procedure to euthanasia of each rat does not exceed 8 min.

The measurement setup used in this study is shown in Figure 11(a), while X-ray fluoroscopy images are provided in Figure 11(b) to illustrate the exact implantation site of the antenna. Measured reflection coefficient frequency responses inside the three different rats under consideration are indicated in Figure 12 (denoted as "rat 1," "rat 2," and "rat 3"). For comparison purposes, numerical results obtained in the "Numerical Design" section are also superimposed (numerical model). Numerical and experimental results are found to exhibit quite good agreement. Compared to numerical simulations, percentage changes in the exhibited resonance frequency ($f_{res}$), reflection coefficient at this frequency ($|S_{11}|_{@fres}$), and 10-dB BW are found to equal +6.9%, +51.9%, and +30.2%, respectively. Maximum deviations in $f_{res}$, $|S_{11}|_{@fres}$, and BW recorded among the three measurements in different rats are found to equal 43 MHz, 12.6 dB, and 23 MHz, respectively.

It is worth noting that other in vivo experimental protocols have also been proposed in the literature for implantable antenna testing inside canine models [54], rats [33], porcine subjects [55], and Göttingen minipigs [56].

## Conclusion

This tutorial provided a simple, yet analytical and complete, step-by-step guide on the numerical design, fabrication, in-vitro, and in-vivo testing of implantable antennas for medical telemetry applications. The tutorial considered an implantable patch antenna for ICP monitoring in the MICS band. Fabrication was performed according to a fabrication procedure, which was optimized based on the available materials and assembling tools. In vitro testing was carried out inside a skin-emulating liquid, whose electrical properties were measured using a dedicated low-cost experimental technique. Finally, in vivo measurements were carried out inside rats, following an in vivo experimentation protocol, which was developed in cooperation with CES-BRFAA. Nevertheless, all steps of this tutorial are applicable to any implantable antenna (type and operating frequency), fabrication procedure, available in vitro materials and equipment, and in vivo experimentation protocol that the designer might have in hand.

## Acknowledgment

This work has been supported by the Operational Program "Education and Lifelong Learning," co-financed by the European Union (European Social Fund-ESF) and national funds, under the project ARISTEIA DEM-II-MED. The work of Asimina Kiourti was supported by the IEEE Microwave Theory and Techniques Graduate Fellowship for Medical Applications. The authors would like to thank Dr. C. Fernandes and Dr. J. Costa for providing the facilities of Instituto de Telecomunicações, Lisbon, Portugal, and helping with in vitro measurements, as well as Dr. N. Kostomitsopoulos for providing the facilities of CES-BRFAA and helping with in vivo measurements.

## References

[1] A. Kiourti, K. A. Psathas, and K. S. Nikita, "Implantable and ingestible medical devices with wireless telemetry functionalities: A review of current status and challenges," *Wiley Bioelectromagn.*, vol. 35, no. 1, pp. 1–15, Jan. 2014.

[2] Z. Tang, B. Smith, J. H. Schild, and P. H. Peckham, "Data transmission from an implantable biotelemeter by load-shift keying using circuit configuration modulator," *IEEE Trans. Biomed. Eng.*, vol. 42, no. 5, pp. 524–528, May 1995.

[3] P. Valdastri, A. Menciassi, A. Arena, C. Caccamo, and P. Dario, "An implantable telemetry platform system for in vivo monitoring of physiological parameters," *IEEE Trans. Inform. Technol. Biomed.*, vol. 8, no. 3, pp. 271–278, Sept. 2004.

[4] "Medical implant communications service federal register," *Rules Regul.*, vol. 64, no. 240, pp. 69926–69934, Dec. 1999.

[5] *IEEE Standard for Local and Metropolitan Area Networks: Wireless Body Area Networks*, IEEE Standard 802.15.6, 2012.

[6] E. Y. Chow, M. M. Morris, and P. P. Irazoqui, "Implantable RF medical devices," *IEEE Microwave Mag.*, vol. 14, no. 4, pp. 64–73, June 2013.

[7] A. Kiourti and K. S. Nikita, "A review of implantable patch antennas for biomedical telemetry: Challenges and solutions," *IEEE Antennas Propagat. Mag.*, vol. 54, no. 3, pp. 210–228, June 2012.

[8] P. Soontornpipit, C. M. Furse, and Y. C. Chung, "Design of implantable microstrip antenna for communication with medical implants," *IEEE Trans. Microwave Theory Tech.*, vol. 52, no. 8, pp. 1944–1951, Aug. 2004.

[9] A. Kiourti and K. S. Nikita, "Miniature scalp-implantable antennas for telemetry in the MICS and ISM bands: Design, safety considerations, and link budget analysis," *IEEE Trans. Antennas Propag.*, vol. 60, no. 6, pp. 3568–3575, Aug. 2012.

[10] C. A. Balanis, *Antenna Theory: Analysis and Design*, 2nd ed. New York: Wiley, 2002.

[11] T. Karacolak, A. Z. Hood, and E. Topsakal, "Design of a dual-band implantable antenna and development of skin mimicking gels for continuous glucose monitoring," *IEEE Trans. Microwave Theory Tech.*, vol. 56, no. 4, pp. 1001–1008, Apr. 2008.
[12] J. Kim and Y. Rahmat-Samii, "Implanted antennas inside a human body: Simulations, designs, and characterizations," *IEEE Trans. Microwave Theory Tech.*, vol. 52, no. 8, pp. 1934–1943, Aug. 2004.
[13] P. Soontornpipit, C. M. Furse, and Y. C. Chung, "Miniaturized biocompatible microstrip antenna using genetic algorithm," *IEEE Trans. Antennas Propag.*, vol. 53, no. 6, pp. 1939–1945, June 2005.
[14] C. J. Sánchez-Fernández, O. Quevedo-Teruel, J. Requena-Carrión, L. Inclán-Sánchez, and E. Rajo-Iglesias, "Dual-band microstrip patch antenna based on short-circuited ring and spiral resonators for implantable medical devices," *IET Microwaves Antennas Propagat.*, vol. 4, no. 8, pp. 1048–1055, Aug. 2010.
[15] J. Kim and Y. Rahmat-Samii, "SAR reduction of implanted planar inverted F antennas with nonuniform width radiator," in *Proc. IEEE Int. Symp. Antennas Propagation*, Albuquerque, NM, July 2006, pp. 1091–1094.
[16] J. Kim and Y. Rahmat-Samii, "Planar inverted F antennas on implantable medical devices: Meandered type versus spiral type," *Microw. Opt. Technol. Lett.*, vol. 48, no. 3, pp. 567–572, Mar. 1996.
[17] W. Huang and A. A. Kishk, "Embedded spiral microstrip implantable antenna," *Hindawi Int. J. Antennas Propag.*, vol. 2011, pp. 1–6, Jan. 2011.
[18] C. M. Lee, T. C. Yo, F. J. Huang, and C. H. Luo, "Bandwidth enhancement of planar inverted-F antenna for implantable biotelemetry," *Microw. Opt. Technol. Lett.*, vol. 51, no. 3, pp. 749–752, Mar. 2009.
[19] N. Vidal, J. M. Lopez-Villegas, S. Curto, J. Colomer, S. Ahyoune, A. Garcia, J. J. Sieiro, and F. M. Ramos, "Design of an implantable broadband antenna for medical telemetry applications," in *Proc. 7th European Conf. Antennas Propagation*, 2013, pp. 1133–1136.
[20] C. M. Lee, T. C. Yo, and C. H. Luo, "Compact broadband stacked implantable antenna for biotelemetry with medical devices," in *Proc. IEEE Annu. Conf. Wireless Microwave Technology*, Clearwater, FL, Dec. 2006, pp. 1–4.
[21] H. Permana, Q. Fang, and I. Cosic, "3-layer implantable microstrip antenna optimized for retinal prosthesis system in MICS band," in *Proc. IEEE Int. Symp. Bioelectronics Bioinformatics*, Nov. 2011, pp. 65–68.
[22] F. J. Huang, C. M. Lee, C. L. Chang, L. K. Chen, T. C. Yo, and C. H. Luo, "Rectenna application of miniaturized implantable antenna design for triple-band biotelemetry communication," *IEEE Trans. Antennas Propag.*, vol. 59, no. 7, pp. 2646–2653, July 2011.
[23] H. Permana, Q. Fang, and W. S. T. Rowe, "Hermetic implantable antenna inside vitreous humor simulating fluid," *Prog. Electromagn. Res.*, vol. 133, pp. 571–590, Jan. 2013.
[24] W. C. Liu, F. M. Yeh, and M. Ghavami, "Miniaturized implantable broadband antenna for biotelemetry communication," *Microw. Opt. Technol. Lett.*, vol. 50, no. 9, pp. 2407–2409, Sept. 2008.
[25] W. C. Liu, S. H. Chen, and C. M. Wu, "Implantable broadband circular stacked PIFA antenna for biotelemetry communication," *J. Electromagn. Waves Applicat.*, vol. 22, no. 13, pp. 1791–1800, 2008.
[26] W. C. Liu, S. H. Chen, and C. M. Wu, "Bandwidth enhancement and size reduction of an implantable PIFA antenna for biotelemetry devices," *Microw. Opt. Technol. Lett.*, vol. 51, no. 3, pp. 755–757, Mar. 2009.
[27] A. Kiourti, M. Tsakalakis, and K. S. Nikita, "Parametric study and design of implantable PIFAs for wireless biotelemetry," in *Proc. 2nd ICST Int. Conf. Wireless Mobile Communication Healthcare*, Kos Island, Greece, Oct. 2011, pp. 96–102.
[28] A. Kiourti, M. Christopoulou, and K. S. Nikita, "Performance of a novel miniature antenna implanted in the human head for wireless biotelemetry," in *Proc. Int. Symp. Antennas Propagation*, Spokane, Washington, July 2011, pp. 392–395.
[29] *IEEE Standard for Safety Levels with Respect to Human Exposure to Radiofrequency Electromagnetic Fields, 3 kHz to 300 GHz*, IEEE Standard C95.1, 1999.
[30] *IEEE Standard for Safety Levels with Respect to Human Exposure to Radiofrequency Electromagnetic Fields, 3 kHz to 300 GHz*, IEEE Standard C95.1, 2005.
[31] A. K. Skrivervik and F. Merli, "Design strategies for implantable antennas," in *Proc. Antennas Propagation. Conf.*, Loughborough, Nov. 2011, pp. 1–5.
[32] J. Abadia, F. Merli, J. F. Zurcher, J. R. Mosig, and A. K. Skrivervik, "3D spiral small antenna design and realization for biomedical telemetry in the MICS Band," *Radioengineering*, vol. 18, no. 4, pp. 359–367, Dec. 2009.
[33] T. Karacolak, R. Cooper, J. Butler, S. Fisher, and E. Topsakal, "In vivo verification of implantable antennas using rats as model animals," *IEEE Antennas Wireless Propag. Lett.*, vol. 9, pp. 334–337, Apr. 2010.
[34] L. Kneisz, M. Schermann, E. Unger, M. Haller, M. Krenn, and W. Mayr, "The short-term effects of antenna insulation thickness on path losses in wireless telemetry implants at microwave frequencies," *Eur. J. Transl. Myol.*, vol. 23, no. 3, pp. 91–94, 2013.
[35] A. Kiourti, J. R. Costa, C. A. Fernandes, A. G. Santiago, and K. S. Nikita, "Miniature implantable antennas for biomedical telemetry: From simulation to realization," *IEEE Trans. Biomed. Eng.*, vol. 59, no. 11, pp. 3140–3147, Nov. 2012.
[36] A. Kiourti and K. S. Nikita, "Recent advances in implantable antennas for medical telemetry," *IEEE Antennas Propagat. Mag.*, vol. 54, no. 6, pp. 190–199, Dec. 2012.
[37] A. Kiourti and K. S. Nikita, "Accelerated design of optimized implantable antennas for medical telemetry," *IEEE Antennas Wireless Propag. Lett.*, vol. 11, pp. 1655–1658, Feb. 2012.
[38] R. Warty, M. R. Tofighi, U. Kawoos, and A. Rosen, "Characterization of implantable antennas for intracranial pressure monitoring: Reflection by and transmission through a scalp phantom," *IEEE Trans. Microwave Theory Tech.*, vol. 56, no. 10, pp. 2366–2376, Oct. 2008.
[39] W. N. Capello, J. A. Dantonio, J. R. Feinberg, and M. T. Manley, "Alternative bearing surfaces: Alumina ceramic bearings for total hip arthroplasty," in *Proc. 10th Symp. Bioceram. Alternative Bearing Joint Arthropl.*, Washington, D.C., June 2005, pp. 87–94.
[40] A. Kiourti and K. S. Nikita, "Miniaturization vs gain and safety considerations of implantable antennas for wireless biotelemetry," in *Proc. Int. Symp. Antennas Propagation*, Chicago, IL, July 2012, pp. 1–2.
[41] C. Gabriel, S. Gabriel, and E. Corthout, "The dielectric properties of biological tissues," *Phys. Med. Biol.*, vol. 41, no. 11, pp. 2231–2293, 1996.
[42] T. Karacolak, R. Cooper, and E. Topsakal, "Electrical properties of rat skin and design of implantable antennas for medical wireless telemetry," *IEEE Trans. Antennas Propag.*, vol. 57, no. 9, pp. 2806–2812, Sept. 2009.
[43] Z. Noroozi and F. Hojjat-Kashani, "Three-dimensional FDTD analysis of the dual-band implantable antenna for continuous glucose monitoring," *Prog. Electromagn. Res. Lett.*, vol. 28, pp. 9–21, 2012.
[44] S. Dey and R. Mittra, "Compact microstrip patch antenna," *Microw. Opt. Technol. Lett.*, vol. 13, no. 1, pp. 12–14, Sept. 1996.
[45] K. L. Wong, C. L. Tang, and H. T. Chen, "A compact meandered circular microstrip antenna with a shorting pin," *Microw. Opt. Technol. Lett.*, vol. 15, no. 3, pp. 147–149, June 1997.
[46] *Ansoft High Frequency Structure Simulator Version 11*, Ansoft Corp., Canonsburg, PA, 2008.
[47] W. Sun and Y. X. Yuan, *Optimization Theory and Methods*. New York: Springer-Verlag, 2006, ch. 5.
[48] *XFDTD, Electromagnetic Solver Based on the Finite Difference Time Domain Method*, Remcom Inc., State College, PA, 2005.
[49] A. Kiourti, J. R. Costa, C. A. Fernandes, and K. S. Nikita, "A broadband implantable and a dual-band on-body repeater antenna: Design and transmission performance," submitted for publication.
[50] K. Ito, K. Furuya, Y. Okano, and L. Hamada, "Development and characteristics of a biological tissue-equivalent phantom for microwaves," *Electron. Commun. Japan*, vol. 84, no. 4, pp. 67–77, 2001.
[51] M. Hofmann, G. Fischer, R. Weigel, and D. Kissinger, "Microwave-based noninvasive concentration measurements for biomedical applications," *IEEE Trans. Microwave Theory Tech.*, vol. 61, no. 5, pp. 2195–2204, May 2013.
[52] F. Merli and A. K. Skrivervik, "Design and measurement considerations for implantable antennas for telemetry applications,"in *Proc. 4th European Conf. Antennas Propagation*, Barcelona, Spain, Apr. 2010, pp. 1–5.
[53] A. Kiourti, K. A. Psathas, P. Lelovas, N. Kostomitsopoulos, and K. S. Nikita, "In vivo tests of implantable antennas in rats: Antenna size and inter-subject considerations," *IEEE Antennas Wireless Propag. Lett.*, vol. 12, pp. 1396–1399, Nov. 2013.
[54] U. Kawoos, M.–R. Tofighi, R. Warty, F. A. Kralick, and A. Rosen, "In–vitro and in–vivo trans–scalp evaluation of an intracranial pressure implant at 2.4 GHz," *IEEE Trans. Microwave Theory Tech.*, vol. 56, pp. 2356–2365, Oct. 2008.
[55] T. Karacolak, R. Cooper, E. S. Unlu, and E. Topsakal, "Dielectric properties of porcine skin tissue and in vivo testing of implantable antennas using pigs as model animals," *IEEE Antennas Wireless Propag. Lett.*, vol. 11, pp. 1686–1689, 2012.
[56] F. Merli, L. Bolomey, F. Gorostidi, B. Fuchs, J. F. Zurcher, Y. Barrandon, E. Meurville, J. R. Mosig, and A. K. Skrivervik, "Example of data telemetry for biomedical applications: An in vivo experiment," *IEEE Antennas Wireless Propag. Lett.*, vol. 11, pp. 1650–1654, 2012.